CHEMISTRY OF MATERIALS

Communication

pubs.acs.org/cm

Mystery of Three Borides: Differential Metal−Boron Bonding Governing Superhard Structures

Paul J. Robinson,[†] Gaoxiang Liu,[‡] Sandra Ciborowski,[‡] Chalynette Martinez-Martinez,[‡] Juan R. Chamorro,[‡] Xinxing Zhang,[‡] Tyrel M. McQueen,[‡] Kit H. Bowen,*[,‡] and Anastassia N. Alexandrova*[,†,§]

[†]Department of Chemistry & Biochemistry, University of California, Los Angeles, Los Angeles, California 90095, United States

[‡]Department of Chemistry and Materials Science, Johns Hopkins University, 3400 N. Charles Street, Baltimore, Maryland 21218, United States

[§]California NanoSystems Institute, Los Angeles, California 90095, United States

Supporting Information

Ultrahard materials have been of interest to human kind since prehistoric times. Borides of certain transition metals form a new class of hard materials.[1−4] Being metals, these borides are easily cut with electric discharge machining and thus appear as an attractive alternative to diamond. The governing principles for the design of ultrahard borides have been proposed to be the combination of high electron density at the Fermi level (E_F) coming from the metal, making borides incompressible, and a rigid covalent boron skeleton resisting the shear stress.[5−10] The metal and boron sublattices in this model are seen independently. Here, we challenge these old principles and show that only with the inclusion of specific metal−boron bonding can we explain and design for the structure and hardness of borides.

We zoom in to a set of three diborides, which are stoichiometrically identical and structurally related yet distinct: TiB_2, ReB_2, and OsB_2 (Figure 1). Among these three, only

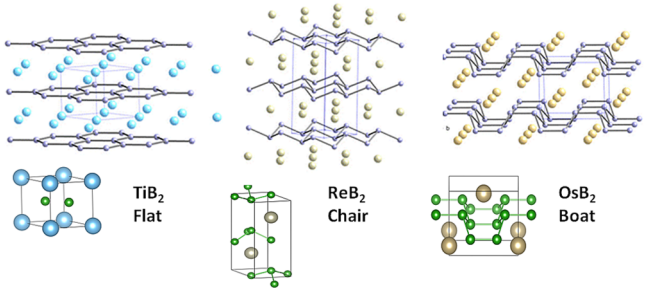

Figure 1. Structures of the three borides: TiB_2 featuring a flat B-sheet and ReB_2 and OsB_2 where the B-sheet is bent in chair and boat conformations, respectively.[1] The upper images display supercells to make apparent the structural analogies while the lower images show a single unit cell.

ReB_2 is ultrahard.[11−13] In all three cases, the boron sublattice is a sheet: planar in TiB_2 and corrugates as a "chair" in ReB_2 and as a "boat" in OsB_2, by analogy with the conformations of cyclohexane. These diborides demonstrate how boron, a metalloid, is capable of many different kinds of bonds to metals, and this promiscuity strongly dictates hardness.

Our approach links the chemical bonding in materials to that in relevant small cluster fragments, which can be studied in great detail using state-of-the-art theory and experiment. The identified critical elements in the electronic structure of the cluster are mapped back onto the solid for property rationalization and design.[14,15]

The most elementary motif that can be observed in the solids is MB_2, and thus, we begin from the $MB_2^{0/-}$ clusters (ions being included for experimental characterization with anion photoelectron spectroscopy). All clusters have C_{2v} symmetry, with the metal coordinating to the center of the B−B bond. However, they have markedly different B−B and M−B distances (see Supporting Information), indicating that metals affect the B−B bonding in different ways. TiB_2^- ($^2A_1$) has a short R(B−B) of 1.56 Å; ReB_2^- has three competing configurations: $^3B_2$, R(B−B) = 1.75 Å; $^3B_1$, R(B−B) = 1.66 Å (2.51 kcal/mol above $^3B_2$); and $^3A_2$, R(B−B) = 1.76 Å (3.14 kcal/mol above $^3B_2$). OsB_2^- ($^4A_2$) has R(B−B) of 1.66 Å. Note that these calculations are large-active-space multireference with dynamic electron correlation (see Supporting Information). This tour de force theoretical approach appeared to be required to reproduce experimental spectra for these seemingly simple systems.[16] The close proximity and mixing of many electronic states can be linked to the promiscuity of metal−boron bonding. Table 1 and Figure 2 show the experimental and theoretical photoelectron spectra (OsB_2^- was not done experimentally due to the high toxicity of Os). The good agreement between theory and experiment signifies that theory can adequately describe these clusters and provide an electronic structure insight.

The chemical bonding in the three neutral clusters (Figure 3) reveals peculiarities of metal−boron interactions and differences between the three clusters. When transition metals interact with B_2, the back-donation first happens to the LUMO of B_2, which is a bonding σ_{2px}-MO. The d-AO → LUMO(B_2) back-donation thus strengthens the B−B bond. The resulting MO falls deep below the HOMO−LUMO gap in ReB_2 and OsB_2, while in TiB_2 it is the HOMO. In addition, Re and Os are capable of back-donation to the LUMO+1 (π^*) of B_2, in the clusters' HOMOs. d → π^* is bonding between the metal and

Received: October 19, 2017
Revised: November 11, 2017
Published: November 14, 2017

DOI: 10.1021/acs.chemmater.7b04378
Chem. Mater. 2017, 29, 9892−9896

Table 1. Experimental and Calculated Photoelectron Spectra of TiB_2^- and ReB_2^- (in eV)

feature	expt. E	transition	calc. E
ReB_2^-			
ADE	0.9 ± 0.1	$^3A_2 \rightarrow {}^4B_1$	1.21
X^1B_3	1.45 ± 0.1	$^3B_1 \rightarrow {}^4B_1$ ($^3B_1$ VDE)	1.51
X^3A_2	1.52 ± 0.1	$^3A_2 \rightarrow {}^4B_1$ ($^3A_2$ VDE)	1.58
A^3B_1	1.65 ± 0.1	$^3B_1 \rightarrow {}^2B_1$	1.70
X^3B_2	1.76 ± 0.1	$^3B_2 \rightarrow {}^4B_1$ ($^3B_2$ VDE)	1.76
TiB_2^-			
ADE	1.4 ± 0.1	$^2A_1 \rightarrow {}^1A_1$	1.09
X	1.68 ± 0.1	$^2A_1 \rightarrow {}^1A_1$ ($^2A_1$ VDE)	1.49
A	1.80 ± 0.1	$^2A_1 \rightarrow {}^3A_1$	1.63
B	1.96 ± 0.1	$^2A_1 \rightarrow {}^1A_1$	1.86
C	2.07 ± 0.1	$^2A_1 \rightarrow {}^3A_1$	2.02

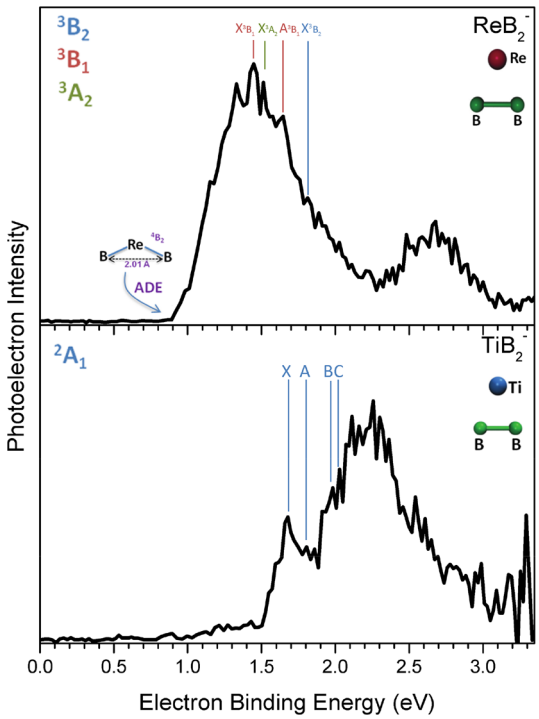

Figure 2. Experimental photoelectron spectra of ReB_2^- (top) and TiB_2^- (bottom) and the theoretical assignment of spectral features.

B_2 and B−B π-antibonding. Due to this MO, R(B−B) in ReB_2 and OsB_2 is elongated. Both back bonds are lower in energy in OsB_2 than in ReB_2, and while this makes little difference for clusters, it will become profoundly important in the corresponding solids. Both types of back bonds are covalent in nature, as seen also from the partial charges on atoms (Figure 3). The ionic M-B_2 bonding component is the strongest in TiB_2. Thus, clusters give us a simple representation of the fundamental M-B_2 interactions possible in the three systems.

In the bulk, the dangling valencies present in clusters are saturated, and so some cluster electronic states become unoccupied. The d → σ_{2px} HOMO in $TiB_2^{0/-}$ does not have an analogue among the valent states in the bulk TiB_2. The material thus exhibits no covalent Ti−B interactions, and the only bonding present is ionic, as is also clear from the charge of +2 on Ti, corresponding to a typical d^2 configuration (Table 2). Furthermore, the +2 charge persists when Ti is substituted into

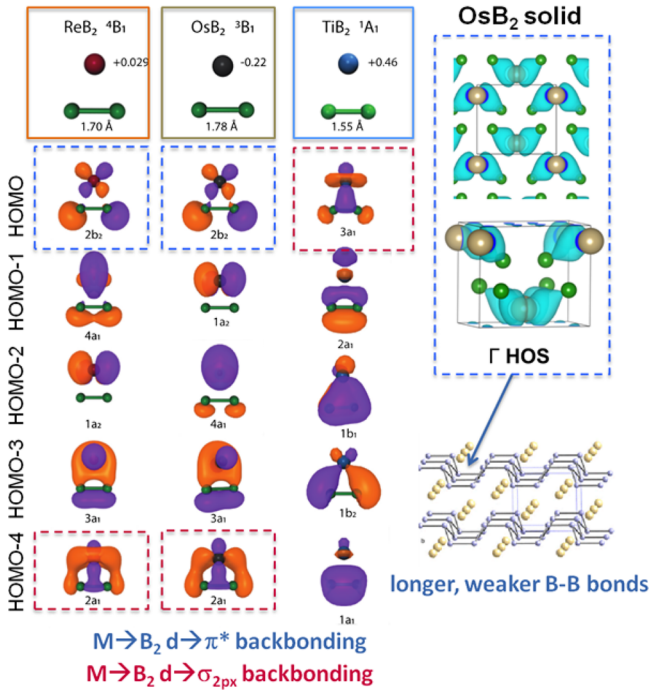

Figure 3. Left: Kohn−Sham orbitals of ReB_2, OsB_2, and TiB_2, truncated set; NBO charges on atoms. The d → σ_{2px} M → B_2 backbonds are outlined in red, and d → π^* in blue. Right: d → π^* state occupied in solid OsB_2 (highest occupied at gamma, HOS), corresponding to the donation from Os to the activated and elongated B−B bonds.

Table 2. Bader Charges of Metals in Both Natural and Foreign Crystal Structures (optimized to the nearest stationary point)

	Os	Re	Ti
boat	**+0.04**	+0.44	+2.02
chair	+0.07	**+0.39**	+1.89
flat	+0.60	+0.93	**+1.98**

the boat or chair structures. The TiB_2 structure type is also characteristic of other diborides including those of Mg, V, Cr, Mn, Sc, Zr, Nb, and Mo.[17] The common electronic origin is the presence of a 2+ metal. M^{+2} means that the boron sublattice receives one electron per B. B^- is isoelectronic to neutral C, and the flat hexagonal boron sheet is therefore isoelectronic and isostructural to graphene. In fact, it has many attributes of graphene, such as the Dirac points.[18]

Both ReB_2 and OsB_2 retain the d → σ_{2px} states in the bulk, in line with their low energies in the cluster models. These states strengthen both M−B and B−B bonding. However, the d → π^* state exists only in OsB_2 and specifically in the longer B−B bonds within the asymmetric "boat" structure (Figure 3). Os has enough electrons to give only half of the B−B bonds a π^* character. Thus, the "boat" structure of OsB_2 is dictated by the antibonding M−B_2 interactions, which makes half of the B−B bonds longer and weaker, while in ReB_2 all B−B bonds are strengthened by M−B interactions. The M−B bonds are stronger in OsB_2. Increased covalent character in Re and Os borides reflects in greatly reduced partial charges as compared to those in TiB_2, particularly in the Os systems (Table 2). Hence we see the chemical bonding origin of the structural differences of the three borides.

DOI: 10.1021/acs.chemmater.7b04378
Chem. Mater. 2017, 29, 9892−9896

We further quantify the degree of covalency and relative bond strengths in the solids via the quantum theory of atoms in molecules (QTAIM) (Figure 4, Table 3), which analyzes the total rather than per-MO charge density.[19,20] QTAIM detects the presence of critical points (CPs) in the charge density. In the "boat" configuration, there are three bond CPs, labeled i (M−B CP), ii (B−B CP), and iii (the second B−B CP). The "chair" structure has two distinct bond CPs, i and ii. The amount of charge at bond CPs correlates with bond strength.[21,22] Both the "boat" and "chair" structures have stronger M−B bonds when containing Os rather than Re. Furthermore, while in general B−B bonds are stronger than M−B bonds, the B−B bonds in the OsB_2 systems are of comparable strength to the Os−B bonds in contrast to the more differentiated ReB_2 systems. Thus, the covalent character of Re/Os−B bonds is confirmed, and it is additionally seen that half of the B−B bonds in OsB_2 are weakened by the interaction with Os, with the charge density flowing from B−B to Os−B bonds.

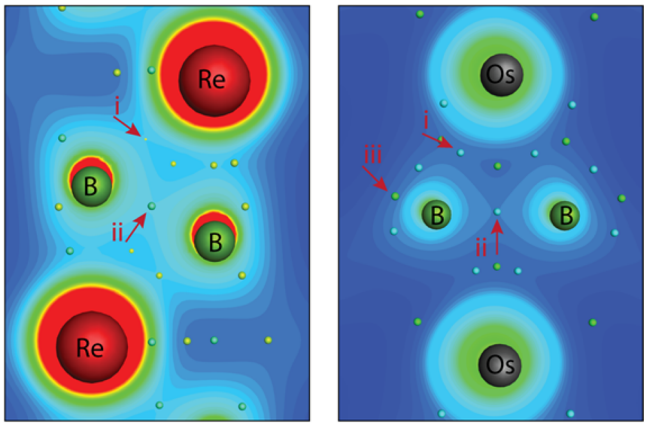

Figure 4. Electron density plots of ReB_2 (left) and OsB_2 (right). QTAIM CPs are indicated: bond CPs, blue; ring CPs, green; cage CPs, yellow. i, M−B CP; ii and iii, B−B CPs.

Table 3. Charge Densities (in e^-) at the Bond CPs for Both Re and Os in the Boat and Chair Structures

	i	ii	iii
ReB_2 boat	0.608	0.740	0.697
OsB_2 boat	0.656	0.732	0.618
ReB_2 chair	0.590	0.713	X
OsB_2 chair	0.629	0.668	X

As a confirmation of the QTAIM analysis, we employed the COHP method to directly measure the bond strengths between the different atoms (see Supporting Information). The integrated COHP values indicate that in ReB_2 Re−B bonds are much weaker than the corresponding B−B bonds, while in OsB_2 Os−B bonds are stronger than the lengthened B−B bonds. This corroborates the QTAIM picture.

There transpires a correlation between the relative strengths of the M−B and B−B bonding and the materials' hardness. In order to pin it down, we depart from the static bonding picture constructed at equilibrium. Hardness is a response to external force, and the effect of pressure is comprised of the combination of two types of distortion: compression and shear. High incompressibility and shear modulus are both necessary but not alone sufficient for hardness.[5−10] We examine the materials' response to these two types of stimuli independently, again relying on the cluster models for clarity.

Because the π^* back bond is not present in the ReB_2 and TiB_2 solids, at this point, the clusters were charged +1 and +2, respectively, in order to unoccupy the d → π^* states. To mimic the effects of compression and shear stress, the B−B compression and M−B_2 shift were applied, and the clusters' responses were monitored (Figure 5).[23] Response to compression should primarily report on the strength of the B−B bonding, whereas that to shear should report on the M−B bonding. The force constants corresponding to the B_2 compression (Figure 5A) show bond stiffening in order of covalent to ionic character. TiB_2^{2+} has the stiffest B−B bond, because it is compact, and electrons confined to the smaller space resist the deformation, while the stable d^2 Ti^{2+} is not willing to relieve the stress by taking electrons back. ReB_2^+, with its d → σ_{2px} back bond, has a strengthened B−B bond and some charge flow toward M−B bonds allowing for the flexibility in charge distribution. Thus, B−B bonds are slightly less stiff than in TiB_2^{2+}. Being the most covalent, Os is the other extreme: the B−B bond activation by the d → π^* donation leads to charge redistribution toward the covalent Os−B bonds. The system is further capable of relieving the stress by shifting electrons toward Os upon the B−B bond compression as if having a shock absorber both in the cluster and in every unit cell in the solid. This reduces the material's stiffness upon compression.

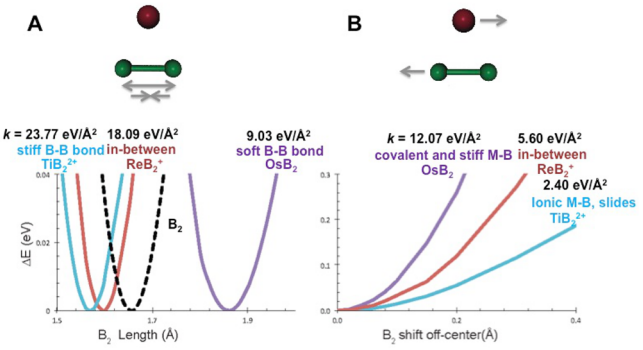

Figure 5. (A) Energies of the clusters as a function of (A) compression along the B−B bond and (B) shear distortion coordinate. Cyan, TiB_2^{2+}; red, ReB_2^+; purple, OsB_2; dashed black, isolated B_2 for a reference.

The clusters' ordering of resistance to shearing is exactly the opposite from that to compressing (Figure 5B). The M−B_2 bonding is the most covalent in OsB_2, intermediate in ReB_2^+, and purely ionic in TiB_2^{2+}. Hence, Ti in TiB_2^{2+} easily slides along B_2, ReB_2^+ resists the slip more, and OsB_2 is the most resilient because the slip disrupts the strong Os−B bonds. OsB_2 has a force constant 5 times higher than that of TiB_2^{2+} for this mode of deformation. To bridge our understanding to the solids, we examine stiffness tensors (Supporting Information Tables 7−11). Starting with compression of the boron network (C_{11}), we see ReB_2 ≈ TiB_2 > OsB_2. This shows the same distinction we had in the clusters: Re and Ti stiffen B the same amount, and Os weakens it. Shearing the metal against the B sheet shows ReB_2 (C_{55}) > TiB_2 (C_{44}) > OsB_2 (C_{66}). This is not the same as the cluster model, but we must consider that there are other interactions in real distortions. The cluster model is Os bound to a long B_2, but in the solid there are also shorter,

DOI: 10.1021/acs.chemmater.7b04378
Chem. Mater. 2017, 29, 9892−9896

more slippery B_2 bonds. Still, it should be hardest to shear on that long B_2 bond in OsB_2 (C_{66}), and that is the case ($C_{66} > C_{44} \gg C_{55}$). In TiB_2 the shear across the B layer is the easiest ($C_{44} < C_{66}$). Thus, we can explain slip-plane strength in solids.

Finally, we computed the geometries and shear moduli of Re and Os in both boat and chair configurations (Table 4). The

Table 4. Calculated Properties of Re and Os in Both the Boat and Chair Structures[a]

	B_2-1 (Å)	B_2-2 (Å)	G (GPa)
OsB_2, boat	1.80	1.88	166
ReB_2, boat	1.84	1.81	244
OsB_2, chair	1.86	X	187
ReB_2, chair	1.82	X	276

[a]G is the shear modulus. X indicates that the structure only has one B_2 bond length.

consequence of more covalent Os−B bonding is a lengthening of the B_2 bonds in the chair structure. This, in turn, lowers the shear modulus. Similarly, Re added to the boat structure causes B_2 bonds to move toward uniformly short, losing the antibonding π^* character, and increasing in the shear modulus. Os in the chair structure is significantly harder than its boat counterpart. This results from forcing the B-lattice to be uniform—no B_2 bond becomes overly covalent, but all are weakened. The moduli thus have full support from the cluster bonding models.

In conclusion, a metal that is too covalent with boron will lower the incompressibility, while a metal that is too ionic with boron will lower the shear strength. A "goldilocks metal" would be intermediate, i.e., having only the bonding d → σ_{2px} and no antibonding d → π^* B−M bonds. Re within the given family of diborides has just the right electron count to fulfill this requirement; as a result ReB_2 is the only ultrahard boride. This constitutes a new bonding model for ultrahard borides, which is based on promiscuous metal−boron bonding, previously unrecognized as one of the crucial aspects of superhard structures. The model reveals the origin of the structural differences in the TiB_2, ReB_2, and OsB_2 borides and explains their differences in hardness. Beyond the three borides, a chemical bonding based design principle for hard materials is a step toward designing novel materials that rival diamond's hardness.

■ ASSOCIATED CONTENT

Supporting Information

The Supporting Information is available free of charge on the ACS Publications website at DOI: 10.1021/acs.chemmater.7b04378.

Theoretical methods, experimental methods, experimental and simulated mass spectra of ReB_2^- and TiB_2^-, alternate minima and excited states of clusters, elastic moduli of structures, elastic tensors of structures, and COHP analysis (PDF)

■ AUTHOR INFORMATION

Corresponding Authors

*K. H. Bowen. E-mail: kbowen@jhu.edu.
*A. N. Alexandrova. E-mail: ana@chem.ucla.edu.

ORCID

Sandra Ciborowski: 0000-0001-9453-4764
Kit H. Bowen: 0000-0002-2858-6352
Anastassia N. Alexandrova: 0000-0002-3003-1911

Author Contributions

P.J.R. and A.N.A. conceived the project and performed the theoretical investigation; G.L., S.C., and K.H.B. designed and carried out the experiments; and C.M.-M., J.R.C., and T.M.M. prepared the rhenium boride rod. P.J.R. and A.N.A. drafted the manuscript. All authors assisted in editing the manuscript.

Notes

The authors declare no competing financial interest.

■ ACKNOWLEDGMENTS

We thank Garth Billings of Diversified Advanced Technologies, LLC (9310 Prototype Drive, Reno, NV 89521, 775-857-4300, garth.billings@sbcglobal.net) for providing the ReB_2 sample. We thank Professor Richard Kaner, Professor Sarah Tolbert, and Dr. Michael Yeung for a helpful discussion. This work was supported by the Air Force Office of Scientific Research (AFOSR) under Grant FA9550-15-1-0259 (K.H.B.), NSF Career Award CHE1351968 (A.N.A.), the Johns Hopkins University Catalyst Fund (T.M.M.), the NSF's PARADIM (Platform for the Accelerated Realization, Analysis, and Discovery of Interface Materials) program, a Materials Innovation Platform (T.M.M.), and the donation of Ms. Evers-Manly for the Undergraduate Research Scholars Program in UCLA (P.J.R.). UCLA IDRE cluster Hoffman2 was used for all calculations.

■ REFERENCES

(1) Chung, H. Y.; Weinberger, M. B.; Levine, J. B.; Kavner, A.; Yang, J. M.; Tolbert, S. H.; Kaner, R. B. Synthesis of Ultra-Incompressible Superhard Rhenium Diboride at Ambient Pressure. *Science* **2007**, *316*, 436−439.

(2) Cumberland, R. W.; Weinberger, M. B.; Gilman, J. J.; Clark, S. M.; Tolbert, S. H.; Kaner, R. B. Osmium Diboride, an Ultra-Incompressible, Hard Material. *J. Am. Chem. Soc.* **2005**, *127*, 7264−7265.

(3) Kaner, R. B.; Gilman, J. J.; Tolbert, S. H. Designing Superhard Materials. *Science* **2005**, *308*, 1268−1269.

(4) Lech, A. T.; Turner, C. L.; Mohammadi, R.; Tolbert, S. H.; Kaner, R. B. Structure Of Superhard Tungsten Tetraboride: A Missing Link Between MB_2 And MB_{12} Higher Borides. *Proc. Natl. Acad. Sci. U. S. A.* **2015**, *112*, 3223−3228.

(5) Levine, J. B.; Tolbert, S. H.; Kaner, R. B. Advancements in the Search for Superhard Ultra-Incompressible Metal Borides. *Adv. Funct. Mater.* **2009**, *19*, 3519−3533.

(6) Gilman, J. J.; Cumberland, R. W.; Kaner, R. B. Design of Hard Crystals. *Int. J. Refract. Hard Met.* **2006**, *24*, 1−5.

(7) Brazhkin, V. V.; Lyapin, A. G.; Hemley, R. J. Harder Than Diamond: Dreams and Reality. *Philos. Mag. A* **2002**, *82*, 231−253.

(8) Haines, J.; Léger, J. M.; Bocquillon, G. Synthesis and Design of Superhard Materials. *Annu. Rev. Mater. Res.* **2001**, *31*, 1−23.

(9) Leger, J. M.; Djemia, P.; Ganot, F.; Haines, J.; Pereira, A. S.; da Jornada, J. A. H. Hardness and Elasticity in Cubic Ruthenium Dioxide. *Appl. Phys. Lett.* **2001**, *79*, 2169−2171.

(10) Harrison, W. A. *Electronic Structure and the Properties of Solids*; Freeman: San Francisco, 1980.

(11) Yeung, M. T.; Mohammadi, R.; Kaner, R. B. Ultraincompressible, Superhard Materials. *Annu. Rev. Mater. Res.* **2016**, *46*, 465−485.

(12) Gu, Q.; Krauss, G.; Steurer, W. Transition Metal Borides: Superhard Versus Ultra-incompressible. *Adv. Mater.* **2008**, *20*, 3620−3626.

(13) Munro, R. G. Material Properties of Titanium Diboride. *J. Res. Natl. Inst. Stand. Technol.* **2000**, *105*, 709−720.

DOI: 10.1021/acs.chemmater.7b04378
Chem. Mater. 2017, 29, 9892−9896

(14) Hoffmann, R. *Solids and surfaces: a chemist's view of bonding in extended structures*; VCH Publishers: 1988.
(15) Hoffmann, R.; Zheng, C. Making and Breaking Bonds in the Solid State: The $ThCr_2Si_2$ Structure. *J. Phys. Chem.* **1985**, *89*, 4175−4181.
(16) Robinson, P. J.; Zhang, X.; McQueen, T.; Bowen, K. H.; Alexandrova, A. N. SmB_6^- Cluster Anion: Covalency Involving f Orbitals. *J. Phys. Chem. A* **2017**, *121*, 1849−1854.
(17) Akopov, G.; Yeung, M. T.; Kaner, R. B. Rediscovering the Crystal Chemistry of Borides. *Adv. Mater.* **2017**, *29*, 1604506.
(18) Feng, X.; Yue, C.; Song, Z.; Wu, Q.; Wen, B. Topological Dirac Nodal-net Fermions in AlB_2-type TiB_2 and ZrB_2. arXiv:1705.00511, 2017.
(19) Morgenstern, A.; Wilson, T.; Miorelli, J.; Jones, T.; Eberhart, M. E. In Search of an Intrinsic Chemical Bond. *Comput. Theor. Chem.* **2015**, *1053*, 31−37.
(20) Bader, R. F. *Atoms in Molecules*; John Wiley & Sons: 1990.
(21) Matta, C. F.; Boyd, R. J. *The Quantum Theory of Atoms in Molecules: From Solid State to DNA and Drug Design*; John Wiley & Sons: 2007.
(22) Grabowski, S. J. Ab Initio Calculations on Conventional and Unconventional Hydrogen Bonds−Study of the Hydrogen Bond Strength. *J. Phys. Chem. A* **2001**, *105*, 10739−10746.
(23) Robinson, P. J.; Alexandrova, A. N. Assessing the Bonding Properties of Individual Molecular Orbitals. *J. Phys. Chem. A* **2015**, *119*, 12862−12867.

DOI: 10.1021/acs.chemmater.7b04378
Chem. Mater. 2017, 29, 9892−9896